Received: 29 August 2018 | Revised: 1 November 2018 | Accepted: 14 November 2018

DOI: 10.1002/aoc.4754

Check for updates

FULL PAPER

WILEY Applied Organometallic Chemistry

The solvent-free synthesis of polysubstituted pyrroles by a reusable copper Schiff base complex immobilized on silica coated Fe_3O_4, and DNA binding study of one resulting derivative as a potential anticancer drug

Jamshid Rakhtshah[1] | Behrooz Shaabani[1] | Sadegh Salehzadeh[2] | Neda Hosseinpour Moghadam[2]

[1] Department of Inorganic Chemistry, Faculty of Chemistry, Tabriz University, Tabriz, Iran

[2] Faculty of Chemistry, Bu-Ali Sina University, Hamedan 6517838683, Iran

Correspondence
Behrooz Shaabani, Department of Inorganic Chemistry, Faculty of Chemistry, Tabriz University, Tabriz, Iran.
Email: shaabani.b@gmail.com

We demonstrate herein the synthesis of a new copper Schiff base complex immobilized on silica-coated Fe_3O_4 nanoparticles. The structure and composition of this magnetic nanocatalyst were analyzed using Fourier transform infrared (FT-IR), X-ray powder diffraction (XRD), vibrating sample magnetometry (VSM), scanning electron microscopy (SEM), energy dispersive X-ray (EDX) and inductively coupled plasma atomic emission spectroscopy (ICP-AES). This nanocomposite was found to be an efficient nanocatalyst for the synthesis of polysubstituted pyrrole derivatives and the products were isolated with high turnover number (TON) and high to excellent yields. Among the new synthesized polysubstituted pyrrole derivatives, we explored the first computational and experimental binding study of methyl 1-benzyl-4-(furan-2-yl)-2-methyl-1H-pyrrole-3-carboxylate (SP-10) with calf thymus deoxyribonucleic acid (ct-DNA), suggesting their application as potential anticancer activity. In addition, the binding modes of SP-10 with DNA and human serum albumin (HSA) were verified by molecular docking technique.

KEYWORDS
DNA binding, immobilized complex, molecular docking, multicomponent reaction, Polysubstituted pyrroles

1 | INTRODUCTION

Transition metal Schiff base complexes have shown high catalytic activities because of the central metal ions in these complexes which easily lend and take electrons from other compounds. The interest in the Schiff base complexes has grown over the past decades.[1–3] Both homogeneous and heterogeneous catalysts of Schiff base complex are important and powerful in the oxidation of organic compounds by various oxygen atom donors.[4–7]

The goal of scientists has lately shifted to alleviate environmental issues; thus, catalyst recovery and reusability have become important aspects of catalytic systems that embrace the principles of green chemistry.[8,9] The major disadvantages of homogeneous catalysts are the difficult separation and regeneration of the expensive catalyst from the catalyst-product mixture at the end of the process. Therefore, to overcome this problem, heterogenization of homogeneous catalysts may combine the ease of catalyst separation with the selectivity of the homogeneous counterparts. Immobilization of the soluble catalyst onto

 © 2018 John Wiley & Sons, Ltd.

various insoluble supports, especially porous materials with high surface areas through the formation of a covalent bond, has been adopted because of easy separation, easy recyclability, thermal stability and long catalytic lifetime.[10–14] Recently, iron oxide magnetic nanoparticles have been found out to be the kind of novel functional materials which are abundant, cheap, environmental friendly and non-toxic.[9] In contrast, immobilized catalysts on Fe_3O_4 can be magnetically recoverable from the reaction mixture by an external magnet. Synthesis, characterization and surface modification of nanoparticles with desired properties have attracted growing attention in recent researches.[10–18]

Pyrroles and their derivatives are extensively found as general core units for various biologically and pharmaceutically active compounds in numerous natural products.[19] There are a number of approaches described in the literature for the synthesis of polysubstituted pyrroles. The preparation of pyrroles can be carried out by four component condensation of aldehydes, amines, ethyl acetoacetate and nitromethane in the presence of various catalysts such as $FeCl_3$,[20] gluconic acid,[21] nano copper oxide,[22] nickel ferrite nanoparticles,[23] β-Cyclodextrin,[24] nano-$CoFe_2O_4$ supported molybdenum,[25] $NiCl_2$,[26] heterogenized tungsten complex,[27] ionic liquid[28] and copper complex immobilized on Fe_3O_4.[29] However, some protocols suffer from certain drawbacks such as high reaction temperature, low yields, prolonged reaction time, tedious workup procedure, low recovery and reusability of the catalyst.

Because of the reasons described above and also as a part of our ongoing research program on the synthesis and characterization of immobilized Schiff base complexes catalysts and their application in multicomponent reactions,[30–33] here, we report an efficient procedure for synthesizing a recoverable and reusable copper Schiff base complex immobilized through a covalent bond linkage on silica-coated magnetic nanoparticles. The successful application of the aforementioned catalyst in the four component reactions for the synthesis of polysubstituted pyrroles at room temperature under solvent free condition has been described (Scheme 1). Also, due to the diverse pharmaceutical properties of the compounds synthesized here, the DNA binding affinity of methyl 1-benzyl-4-(furan-2-yl)-2-methyl-1H-pyrrole-3-carboxylate (SP-10) as a new derivative was investigated by using molecular docking simulations as well as UV–vis spectroscopy and viscometry method.

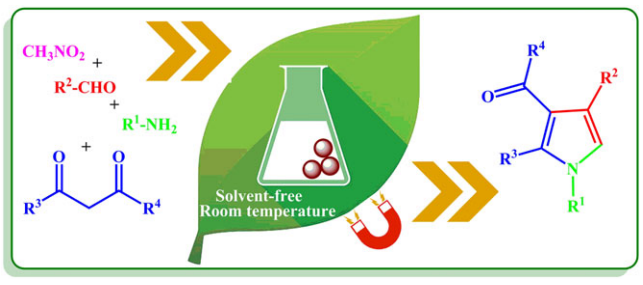

SCHEME 1 The synthesis of pyrrole derivatives using copper complex supported on functionalized Fe_3O_4 magnetite nanoparticles

2 | EXPERIMENTAL

2.1 | Materials and characterization techniques

All chemicals were purchased from Merck, Fluka or Aldrich and used without any further purification. The particle size and morphology were investigated by SEM using FESEM-TESCAN MIRA3. FT-IR measurements were performed using the KBr disc on a Perkin–Elmer FT-IR spectrometer 17259. The XRD patterns of samples were recorded on a D8 Advanced diffractometer (Bruker AXS Inc., 40 kV, 30 mA) X-ray diffractometer. Scans were taken with a 2θ and step size of 0.02 from 20–80° and a counting time of 1.0 s using a Cu Kα radiation source (λ = 1.542 Å) to assess the crystallinity. VSM measurement was recorded by a magnetometer (VSM-4 inch; Daghigh Meghnatis Kashan, Kashan, Iran) at room temperature. The copper content of the catalyst was determined using an ICP-AES instrument (HORIBA Jobin Yvon, Longjumeau Cedex, France). UV–vis spectroscopy was conducted by UV Win T80 spectrophotometer.

The procedure for synthesis of copper Schiff base complex supported on Fe_3O_4 nanoparticles includes four steps, schematically illustrated in Scheme 2.

2.2 | General procedure for the synthesis of copper Schiff base complex (CuSB)

2-Formylpyridine (0.5 g) was added to a magnetically stirring solution of 4-aminophenol (0.5 g) in ethanol (40 ml). After refluxing for 3 hr, the mixture was cooled to room temperature. The resulting crystals were separated by filtration, washed with ethanol and dried under vacuum. Then, an ethanol (10 ml) solution of copper acetate (1.81 g, 10 mmol) was added dropwise to an ethanol solution (10 ml) of prepared Schiff base ligand (1.98 g, 10 mmol) and the mixture was refluxed for 2 hr. The resulting crystalline solid was separated and filtered off, then washed with ethanol (3 × 5 ml) to give copper Schiff base complex (Yield: 85%).

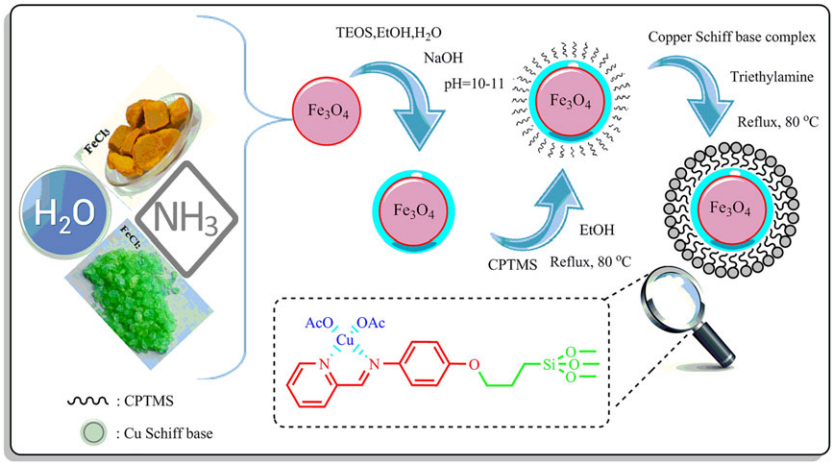

SCHEME 2 The sequence of events in the preparation of Fe_3O_4@SiO_2@CuSB

2.3 | Synthesis of immobilized copper Schiff base complex on magnetic iron oxide nanoparticles (Fe_3O_4@SiO_2@CuSB)

Firstly, preparation of naked Fe_3O_4 was carried out according to the previously reported method.[34] A mixture of $FeCl_3.6H_2O$ (2 mmol, 7.8 g) and $FeCl_2.4H_2O$ (1 mmol, 2.9 g) was dissolved in 110 ml deionized water at 80 °C, then after stirring for 10 min, a 25% NH_4OH solution (90 ml) was added quickly to the resulting solution in one portion with vigorous mechanical stirring. After cooling to room temperature, the black precipitates were collected using an external magnet. The magnetic nanoparticles were washed with deionized water and a solution of NaCl (10%wt) through magnetic decantation. Secondly, silica coated Fe_3O_4 nanoparticles (Fe_3O_4@SiO_2) were prepared by Stober method[35] with slight modification. The obtained magnetic nanoparticles (MNPs) (1 g) were dispersed in 220 ml ethanol/water (volume ratio, 10:1) solution by sonication for 10 min, and then 4 ml of tetraethylorthosilicate (TEOS) was added dropwise to the mixture. After mechanical stirring in 60 °C under N_2 atmosphere for 6 hr, the silica coated nanoparticles were collected using a magnet and washed with ethanol to remove remnant of compound. Thirdly, Fe_3O_4@SiO_2 (1 g) was added to the solution of 3-chloropropyltrimethoxysilane (CPTMS) (2 ml) in ethanol (50 ml) and the resultant mixture was kept at 80 °C under reflux and N_2 atmosphere for 12 hr. Practically, the ethanol solution deleted the excess amount of Si-linker, providing a better and faster decantation of suspended Fe_3O_4 nanoparticles in ethanol, when an external magnet was used. Finally, chloropropyl coated nanoparticles (0.5 g), triethylamine and synthesized copper Schiff base complex (0.5 g) were added to ethanol (50 ml). The resulting mixture was stirred for 3 hr and then the precipitates were collected using an external magnet and washed with ethanol and also distilled water for three times. The solid was dried at 60 °C in oven for 12 hr.

2.4 | General procedure for the synthesis of polysubstituted pyrrole derivatives (SP)

To a 50 ml round-bottomed flask reactor were added various amines (1 mmol), different aldehydes (1 mmol), ethyl acetoacetate (1 mmol), nitromethane (1 mmol) and Fe_3O_4@SiO_2@CuSB as catalyst (6 mg) sequentially. The suspension was stirred vigorously at room temperature followed by an appropriate time of stirring in solvent-free condition. The progress and completion of the reaction was monitored by thin layer chromatography (TLC) (n-hexane/ethyl acetate (5:3)). After the reaction completion, the mixture was diluted with dichloromethane (3 ml) and stirred at high temperature. Finally, the catalyst was separated by magnetic decantation from resulting mixture. After evaporation of the solvent, the crude product was recrystallized with ethanol to give a pure product. All new compounds were characterized by IR, ^1H and ^{13}C NMR spectroscopy (supporting information).

2.5 | Molecular docking

The structure of methyl 1-benzyl-4-(furan-2-yl)-2-methyl-1H-pyrrole-3-carboxylate (SP-10) was optimized at DFT (BP86) level of theory.[36,37] The def2-TZVP[38] basis set was employed for all atoms, and the structure was optimized without symmetry restrictions. All calculations were performed using the Gaussian 03 set of programs.[39] The optimized structure of SP-10 was used for the molecular docking calculations (Figure 1). The crystal structures of all the pdb DNA and HSA used in molecular

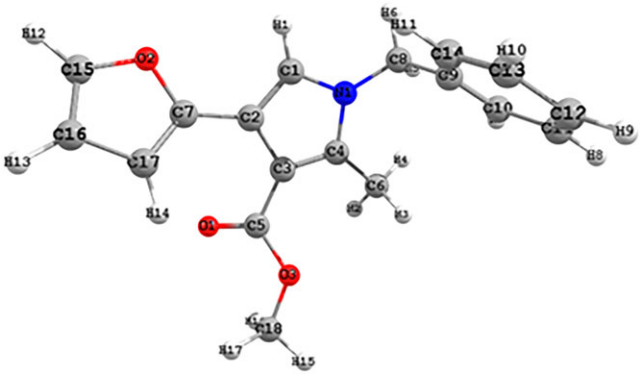

FIGURE 1 The optimized structure of methyl 1-benzyl-4-(furan-2-yl)-2-methyl-1H-pyrrole-3-carboxylate (SP-10)

docking were extracted from Protein Data Bank (http://www.rcsb.org/pdb/home/home.do) and listed in Table 1.

The binding interactions of SP-10 with all of the pdb DNA structures and HSA were simulated by molecular docking method using AutoDock 4.0 program.[40] All of the water molecules were removed from all pdb structures. The polar hydrogen atoms were added to all of the pdb structures. The grid maps of dimensions $60 \times 60 \times 60$ A° and $126 \times 126 \times 126$ A° with a grid-point spacing of 0.375 A° were created respectively for five DNA structures and HSA to ensure an appropriate size for X-accessible space. Also the values of the centers of grid boxes are shown in Table 1. Other miscellaneous parameters were assigned to the default values given by the Autodock program. Finally, we obtained the dominating configuration of the binding complex of SP-10 with five DNA structures and HSA with minimum binding free energy (ΔG).

2.6 | UV–visible absorption spectral measurements

The concentration of drug candidate was fixed at 5×10^{-5} M and the ct-DNA concentration varied from 0 to 9.6×10^{-5} M. Control samples consisted of only ct-DNA solution. The spectra were recorded in the range of 220–440 nm at room temperature.

2.7 | Viscosity measurements

Viscometric measurements were carried out using a viscometer which was kept at 25 ± 0.2 °C by a constant temperature bath. The solution of (DNA + SP-10) was prepared in Tris–HCl buffer and the flow times of ct-DNA alone and its mixtures with different ratios of SP-10 to ct-DNA through the capillary were then measured in three replicates using a digital stopwatch with an accuracy of ±0.02 s. The data were presented as $(\eta/\eta_0)^{1/3}$ versus the ratio of the concentration of compound to that of DNA, where η and η_0 are the viscosity of DNA in the presence and absence of our derivative, respectively.

2.8 | Circular dichroism (CD) studies

The CD measurements were recorded on a JASCO (J-810) spectropolarimeter, using a 1.0 cm quartz cell by keeping the concentration of DNA at 8×10^{-5} M and various concentrations of SP-10.

TABLE 1 Five DNA sequences and HSA used for molecular docking[a]

ID	PDB ID	Sequences	Unit Cell constants	Centers of grid boxes
1	1BNA	D $(CGCGAATTCGCG)_2$	a = 24.87 Å, b = 40.39 Å, c = 66.20 Å α = 90 °, β = 90 °, γ = 90 °	14.719, 20.979, 8.824
2	1D32	D $(CGCG)_2$	a = 16.88 Å, b = 26.88 Å, c = 82.60 Å α = 90 °, β = 90 °, γ = 90 °	26.699, 13.011, 10.343
3	1DNE	D $(CGCGATATCGCG)_2$	a = 25.48 Å, b = 41.26 Å, c = 66.88 Å α = 90 °, β = 90 °, γ = 90 °	15.259, 21.297, 75.998
4	1K2J	D $(CGTACG)_2$	No data	0.218, 1.887, 7.463
5	1ZNA	D $(CGCG)_2$	a = 31.27 Å, b = 64.67 Å, c = 19.50 Å α = 90 °, β = 90 °, γ = 90 °	18.079, −8.217, 8.853
6	1AO6	HSA	a = 59.68 Å, b = 96.98 Å, c = 59.72 Å α = 91.07 °, β = 103.50 °, γ = 75.08 °	29.535, 31.826, 23.5

[a]These data were extracted from Protein Data Bank (http://www.rcsb.org/pdb/home/home.do).

3 | RESULTS AND DISCUSSION

3.1 | Characterization of copper Schiff base complex immobilized on silica-coated iron oxide nanoparticles as a heterogeneous catalyst

All the evidence from Fourier transform infrared (FT-IR) spectroscopy, X-ray diffraction (XRD), field emission scanning electron microscopy (FE-SEM), energy-dispersive X-ray spectroscopy (EDS), inductively coupled plasma (ICP) and vibrating sample magnetometry (VSM) analyses support the successful grafting of copper Schiff base complex onto the surface of silica coated magnetic nanoparticles.

FT-IR spectra of the Fe_3O_4, $Fe_3O_4@SiO_2$, $Fe_3O_4@SiO_2@Cl$, $Fe_3O_4@SiO_2@CuSB$ and Cu Schiff base complex are shown in Figures 2a, 2b, 2c, 2d and 2e, respectively. The strong absorption signal observed at 570 cm^{-1} is attributed to the Fe-O bond stretching vibration. The broad band at 3000–3500 cm^{-1} is referred to the absorption of –OH stretching of surface hydroxyl groups.[41] The introduction of silica layer to the surface of naked Fe_3O_4 is confirmed by the sharp band at 1078 cm^{-1} assigned to the Si-O-Si anti-symmetric stretching vibration.[42] The synthesized $Fe_3O_4@SiO_2@Cl$ possesses the main peak at 2840 to 2918 cm^{-1} which indicates the presence of the anchored propyl group of CPTMS on magnetic NPs by C–H stretching vibrations.[41] Reaction of CPTMS coated nanoparticles with copper Schiff base produces $Fe_3O_4@SiO_2@CuSB$ in which the presence of imine stretching band is asserted with 1628 cm^{-1} bands in Figure 2(d) spectra. Also, in IR spectra of neat copper Schiff base, the vibrational stretching frequency of C=N bond appears at 1628 cm^{-1}.[30]

The structure and phase purity of the Fe_3O_4 (3a) and $Fe_3O_4@SiO_2@CuSB$ (3b) were examined by XRD. The obtained materials had similar diffraction peaks at $2\theta = 30, 35, 43, 53, 62$ and 74°, which could be indexed to an inverse spinel ferrite of Fe_3O_4 (JCPDS file number 89–3854).[43] Eight peaks in XRD patterns correspond to Miller indices value (hkl) of (220), (311), (400), (422), (511) and (440), respectively.[32] In addition, no specific peaks due to any impurities were observed and the copper species is highly dispersed on nanoparticles. Figure 3b presents almost the same feature as the one shown in Figure 3a, which is attributed to the fact that surface modification of the nanoparticles does not lead to their phase change. According to the Scherrer equation[44] based on the full width at half-maximum (FWHM) of main diffraction peak, the mean crystallite size of synthesized nanocrystals is estimated to be about 30 nm. Also, the XRD pattern of reused catalyst (Figure 3c) shows that the Fe_3O_4 phase has not been changed during the catalytic reaction.

In order to investigate the morphology of the $Fe_3O_4@SiO_2@CuSB$, SEM images of the magnetic nanoparticles were provided and the images are presented in Figure 4. As it is clear, the copper complex immobilized on Fe_3O_4 exhibits a cluster of aggregated spherical particles. The EDS pattern of elements in nanomaterial confirms the presence of Fe, O, Si, N, C, Cl and Cu species in the structure of catalyst.

The superparamagnetic property of Fe_3O_4 and $Fe_3O_4@SiO_2@CuSB$ was investigated by vibrating sample magnetometer (VSM) at room temperature. As shown from the loops in Figure 5, the saturation magnetization (M_S) of naked magnetic nanoparticles and immobilized complex on magnetic nanoparticles are 48.85 and 40.27 emu g^{-1}, respectively. The decrease in the magnetization value of the composite in comparison with Fe_3O_4 NPs is due to the immobilizing of silica layer and Schiff base complex of copper on Fe_3O_4 nanoparticles through their bond formation via their hydroxyl functional groups.[45] Nonetheless, the synthesized catalysts in this study had a sufficient superparamagnetic behavior and

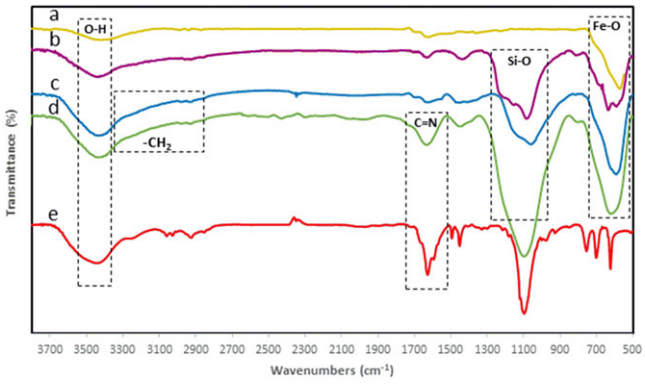

FIGURE 2 FT-IR spectra of Fe_3O_4 (a), $Fe_3O_4@SiO_2$ (b), $Fe_3O_4@SiO_2@Cl$ (c), $Fe_3O_4@SiO_2@CuSB$ (d), neat copper Schiff base complex (e)

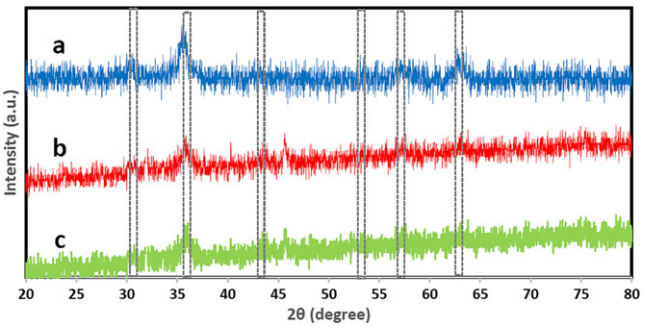

FIGURE 3 Powder XRD patterns of Fe_3O_4 (a), $Fe_3O_4@SiO_2@CuSB$ (b) and reused $Fe_3O_4@SiO_2@CuSB$

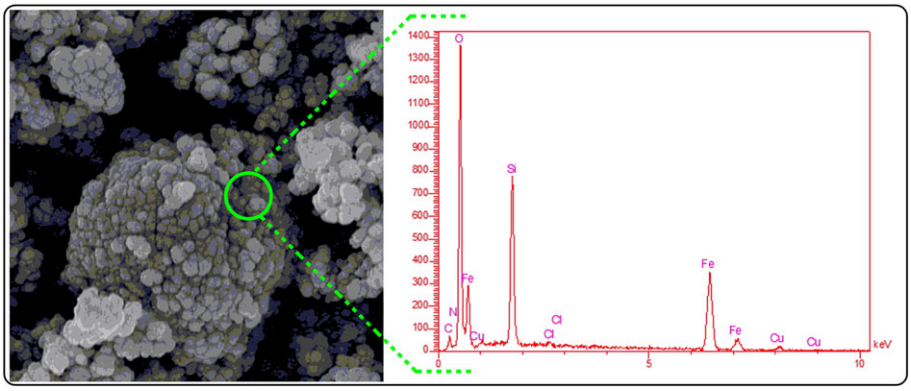

FIGURE 4 FE-SEM micrograph with the scale bar of 500 nm and EDX spectrum of Fe_3O_4@SiO_2@CuSB

thus, they still could be readily separated from reaction mixture with the aid of an external magnet.

Also, in order to determine the amount of copper content of the catalyst, ICP analysis was performed and it was found to be 0.34 mmol g^{-1}.

3.2 | Application of copper Schiff base complex immobilized on silica coated iron oxide nanoparticles as a heterogeneous catalyst

Polysubstituted pyrroles have widespread uses due to their significant biological activity. Thus, our studies were directed towards the possibility of applying magnetic nanoparticles to the design of an efficient, recyclable and magnetically recoverable heterogeneous catalyst for the synthesis of polysubstituted pyrroles under mild reaction conditions. For initial optimization of the reaction conditions and the identification of the best amount of the catalyst at different temperatures, aniline, benzaldehyde, ethyl acetoacetate and nitromethane were chosen as model substrates. In order to show the role of the catalyst, similar reactions in the absence and also in the presence of different amounts of catalyst were examined.

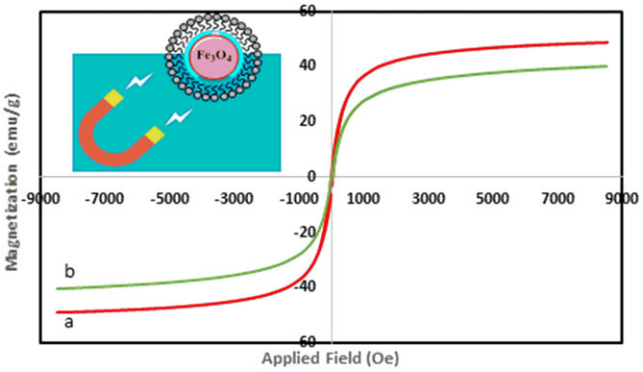

FIGURE 5 Magnetic hysteresis curves measured at room temperature for Fe_3O_4 (a) and Fe_3O_4@SiO_2@CuSB (b)

In the absence of nanocatalyst, the reaction did not proceed with good yield even after a long reaction time (Table 2, entries 1–2). It was found that at a higher amount, the catalyst performed in shorter reaction times (Table 2, entries 1–5). By screening different amounts of the catalyst (2, 4, 6, 8 mg) at room temperature, pyrroles were afforded with 45%, 75%, 94%, and 94% isolated yields, respectively. Therefore, the best yield is observed

TABLE 2 The effect of amount of the catalyst and temperature on the four-component reaction under solvent-free conditions[a]

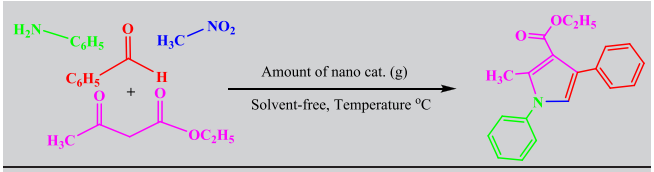

Entry	Amount of catalyst (mg)	Reaction temperature (°C)[b]	Reaction time (min)	Yield[c] (%)
1	—	r.t.	45	30
2	—	100	45	30
3	2	r.t.	45	45
4	2	100	45	50
5	4	r.t.	45	75
6	4	100	45	77
7	6	r.t.	20	94
8	6	50	20	94
9	6	75	20	94
10	6	100	20	94
11	8	r.t.	20	94
12	8	100	20	94

[a]Reaction conditions: benzaldehyde (1 mmol), aniline (1 mmol), ethyl acetoacetate (1 mmol) and nitromethane (1 mmol).

[b]This is the temperature of oil bath and not inside the reaction medium.

[c]Isolated yield.

TABLE 3 Solvent effect on the four-component reaction[a] at room temperature using 6 mg catalyst

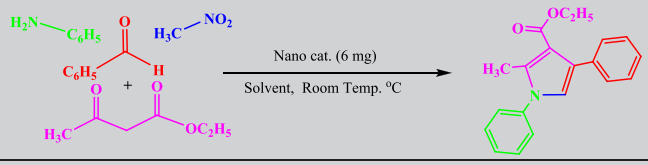

	Solvent-free	H_2O	C_2H_5OH	CH_3CN	CH_2Cl_2	Toluene	*n*-Hexane
Yield (%)[b]	94	35	70	60	50	30	35
Reaction time (min)	20	40	45	40	35	50	60

[a]Benzaldehyde (1 mmol), aniline (1 mmol), ethyl acetoacetate (1 mmol) and nitromethane (1 mmol) under room temperature;

[b]Isolated yield.

in the presence of just 6 mg nanocatalyst, and the higher amounts of catalyst than this does not improve the yield (Table 2, entries 11–12). We next investigated the effect of different temperatures (25, 50, 75 and 100 °C) on the reaction rate as well as the yields of products. The best results were obtained at room temperature and higher temperatures did not improve the yield or reaction rate in the same amount of catalyst (Table 2, entries 7–10). Then, the effect of various solvents and solvent-free conditions on the model reaction was screened. As shown in Table 3., we found that using solvent-free condition, compared with other solvents, in the presence of magnetite nanoparticles, the desired product with high yield and shorter reaction time will be obtained.

To survey the efficiency of the procedure, we studied the catalytic performance of the immobilized copper Schiff base complex on magnetic nanoparticles in one-pot four-component condensation of different amines, various aromatic aldehydes, ethyl acetoacetate and nitromethane for the preparation of corresponding polysubstituted pyrrole derivatives. From the experiments mentioned above, the optimum condition (6 mg of the catalyst under solvent-free conditions at room temperature) was chosen. The reaction can tolerate a wide range of aromatic aldehydes bearing halogens, heterocyclic, electron-donating and electron withdrawing substituents in the ortho, meta and para positions. Representative results are summarized in Table 4. All of these reactions proceed rapidly and they are completed in the range of 20–40 min. Aldehydes with electron-donating groups are less active than those with electron-withdrawing groups in the para-positions. All products were prepared in the short reaction time and in high to excellent yields. Furthermore, we calculated turnover numbers (TONs) and turnover frequencies (TOFs) (according to the ICP results, 6 mg of catalyst is equivalent to 0.204 mol% of catalyst) states on the effectiveness of these catalysts. The results are summarized in Table 4. The new products were characterized by IR, ^{1}H NMR and ^{13}CNMR spectroscopy, and also by comparison of their spectroscopic data with those reported in the literature.

To compare the catalytic activity of the new catalyst with previously known ones, we evaluated the catalytic activity of these catalysts in the model reaction under different conditions. Table 5 shows that our catalyst has efficiently catalyzed the model reaction to give the desired product in excellent yield and relatively shorter reaction time among all catalysts.

For investigations on the recyclability of heterogeneous system, the lifetime of the catalyst was studied (Figure 6). After the first use of nanocatalyst in the model reaction to give the desired product in quantitative yield, ethyl acetate was added to the reaction mixture and stirred and heated to separate the product. More than 99% of the catalyst could simply be recovered by using a magnet near to the reaction medium, and the catalyst was magnetically separated and washed thoroughly with ethanol. A new reaction was then performed with fresh reactants under the same conditions. Surprisingly, the recovered catalyst at each reaction was reused without significant deactivation even after ten times reuse of catalyst. We believe that this is also the possible reason for the high reusability of the catalyst presented herein. The amount of leached copper in the final product was measured by the ICP technique. No Cu metal was detected after completion of the reaction which confirms the fact that Schiff base provides enough binding sites on the surface of silica coated magnetic nanoparticles and serves as a preventing metal leaching, and enabling efficient catalyst recycling.

3.3 | Molecular docking study of SP-10 as a potential anticancer activity

Computational molecular docking is a valuable method for predicting the stable structure of receptor-ligand complex for better diagnosis of the interaction details in the drug discovery process.[46,47] This technique is often used

TABLE 4 Four-component reaction for synthesis of polysubstituted pyrrole derivatives using 6 mg catalyst under solvent-free condition[a]

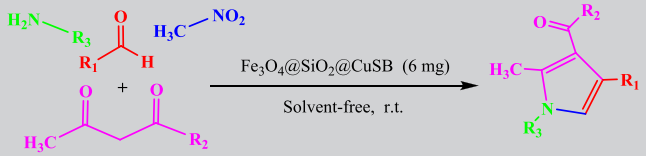

Name	Product	Time (min)	Yield[b] (%) (g)	TON	TOF (min^{-1})	M.p (°C) [Lit.]
SP-1	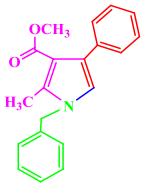	20	94 (0.287)	460.8	23.1	Oil[27]
SP-2	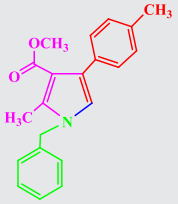	30	85 (0.271)	416.7	13.9	Oil[23]
SP-3	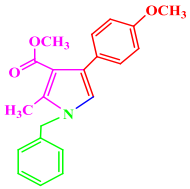	35	85 (0.285)	416.7	11.9	Oil[27]
SP-4	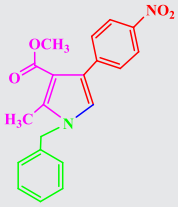	20	91 (0.318)	446.0	22.3	Oil[23]
SP-5	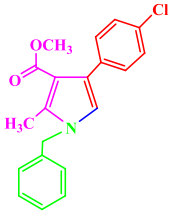	30	90 (0.305)	441.2	14.7	Oil[23]

(Continues)

TABLE 4 (Continued)

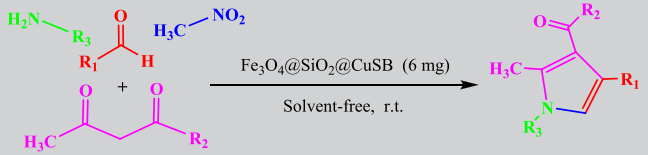

Name	Product	Time (min)	Yield[b] (%) (g)	TON	TOF (min^{-1})	M.p (°C) [Lit.]
SP-6	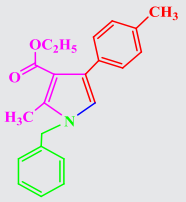	25	90 (0.300)	441.2	17.6	Oil[27]
SP-7	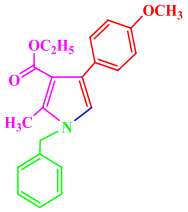	30	80 (0.279)	392.2	13.1	Oil[22]
SP-8	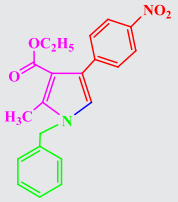	25	95 (0.346)	465.7	18.6	Oil[22]
SP-9	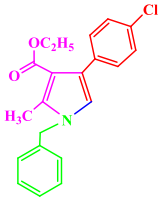	30	92 (0.325)	450.1	15.1	Oil[23]
SP-10	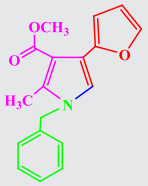	30	94 (0.277)	460.8	15.4	115–117 °C [c]

(Continues)

TABLE 4 (Continued)

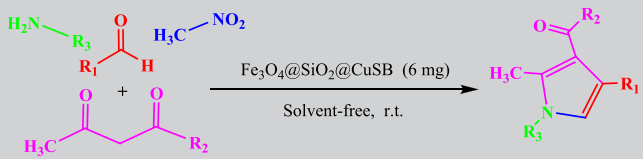

Name	Product	Time (min)	Yield[b] (%) (g)	TON	TOF (min^{-1})	M.p (°C) [Lit.]
SP-11	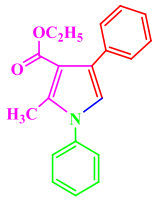	20	94 (0.287)	460.8	23.1	Oil[28]
SP-12	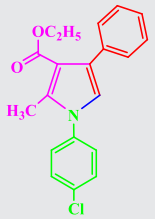	30	90 (0.305)	441.2	14.8	108–110 °C[29]
SP-13	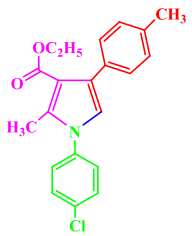	25	85 (0.300)	416.7	16.7	127–129 °C[29]
SP-14	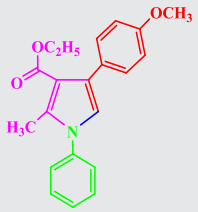	35	90 (0.301)	441.2	12.1	120–122 °C[29]

[a]: Reaction conditions: different aldehydes (2 mmol), different amines (2 mmol), ethyl acetoacetate (2 mmol), nitromethan (2 mmol), nano catalyst (6 mg), solvent free and room temperature.

[b]: Isolated yield.

[c]: New derivative.

TABLE 5 Comparison of the Fe_3O_4@SiO_2@CuSB catalytic activity with those of reported catalysts[a]

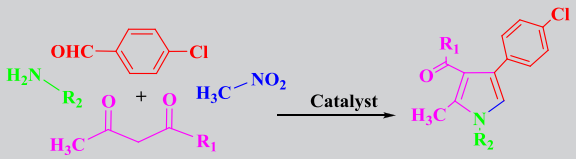

Catalyst	Solv.	Temp (°C)	Time (min)	Yield[b] (%)	R_1	R_2	[Ref.]
Amberlyst-15	-	r.t.	30	80	OMe	$C_6H_5CH_2$	[19]
$FeCl_3$	-	Reflux	420	80	OMe	$C_6H_5CH_2$	[20]
Nano Copper oxide	-	100–105	720	78	OMe	$C_6H_5CH_2$	[22]
Heterogenized Tungsten Complex	-	Reflux	270	85	OMe	$C_6H_5CH_2$	[27]
Nickel (II) chloride hexahydrate	-	r.t.	480	78	OMe	$C_6H_5CH_2$	[26]
Nickel ferrite nanoparticles	-	100	240	96	OMe	$C_6H_5CH_2$	[23]
Fe_3O_4@SiO_2@SBCu	-	r.t.	25	90	OMe	$C_6H_5CH_2$	[29]
Fe_3O_4@SiO_2@CuSB		r.t.	20	94	OMe	$C_6H_5CH_2$	-

[a]Model reaction: benzaldehyde, aniline, ethyl acetoacetate and nitromethane;

[b]Isolated yield.

as a virtual searching tool in the early stages of drug design and development. In the present work, in order to find out the preferred location of SP-10 on DNA and HSA, molecular docking studies were carried out using Autodock 4.0. Furthermore, to determine the preferential binding sites of SP-10 on different types of DNA, the SP-10 was docked into various types of rigid DNA and the results were listed in Table 5 (Figure 7.). The values of electrostatic forces between SP-10 and DNAs is much lower than the sum of van der Waals energy, hydrogen bonding energy and desolvation free energy in the binding process, indicating that the main binding mode between SP-10 and DNAs is not electrostatic.

In order to obtain a deep insight into the SP-10 binding mode with HSA, computational molecular docking has been employed and the possible conformations of the protein-(SP-10) complex were calculated. Among the possible conformers, the conformer with the lowest binding free energy was used for further analyses. From the crystal structure of human serum albumin (HSA), it can be concluded that HSA is a heart-shaped protein consisting of a single polypeptide chain of 585 amino acid residues.[48] Each of the structurally similar α-helix domains (I–III) has two subdomains (A and B), with six α-helices in subdomain A and four α-helices in subdomain B.[49] Figure. 8 shows the most possible binding mode between SP-10 and HSA and clearly indicates

TABLE 6 The various energies and the hydrogen bonding interactions in the formation process of DNAs-(SP-10) and HSA-(SP-10) complexes

PDB ID	$\Delta G^0_{(a)}$ kcal mol^{-1}	$\Delta E_{1(b)}$ kcal mol^{-1}	$\Delta E_{2(c)}$ kcal mol^{-1}	Hydrogen bonding			Binding site
				DNA	Met	Bond length (Å)	
1BNA	−6.55	−8.04	+0.02	No hydrogen bonds formed			Major groove
1D32	−6.74	−8.23	−0.11	No hydrogen bonds formed			Intercalation
1DNE	−7.75	−9.24	−0.09	No hydrogen bonds formed			Minor groove
1K2J	−6.29	−7.78	−0.04	G6:H22 (Chain A) G8:H3 (Chain B)	O2 C5 = O1	1.914 1.701	Major groove
1ZNA	−6.65	−8.14	−0.23	G2:H22 (Chain A)	O2	2.223	Major groove
104D	−6.04	−7.53	+0.02	C15:H42 (Chain B)	O2	2.034	Major groove
1AO6	−7.94	−9.43	−0.12	VAL482(NH) (Chain A)	O2	1.828	IIA

(a) ΔG^0 is the binding free energy changes in the binding process. (b) ΔE_1 denotes intermolecular interaction energy, which is a sum of van der Waals energy, hydrogen bonding energy, desolvation free energy and electrostatic energy. (c) ΔE_2 is the electrostatic energy

FIGURE 6 Reusability of Fe_3O_4@SiO_2@CuSB as a heterogeneous catalyst

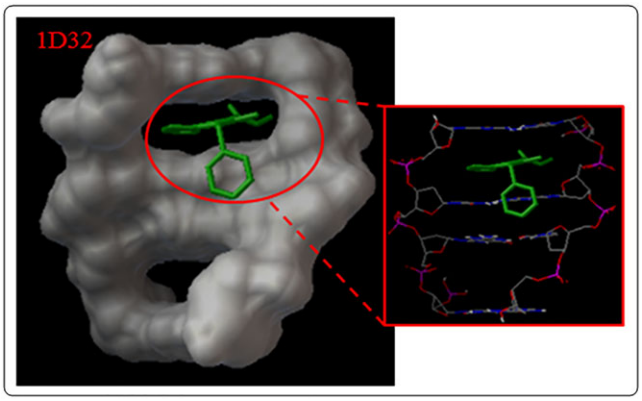

FIGURE 7 Molecular docking of the interaction of 1D32 as a type of DNA with SP-10

that SP-10 is located in the site I subdomain IIA, and was stabilized by the formation of a hydrogen bond with Val 482 in the system. Moreover, SP-10 was in the locality of some hydrophobic residues of HSA (site I subdomain IB),[50] which suggested the existence of hydrophobic interaction between it and HSA. This means that hydrogen bonding and hydrophobic interactions play an important role in the stability of HSA-(SP-10) complex.

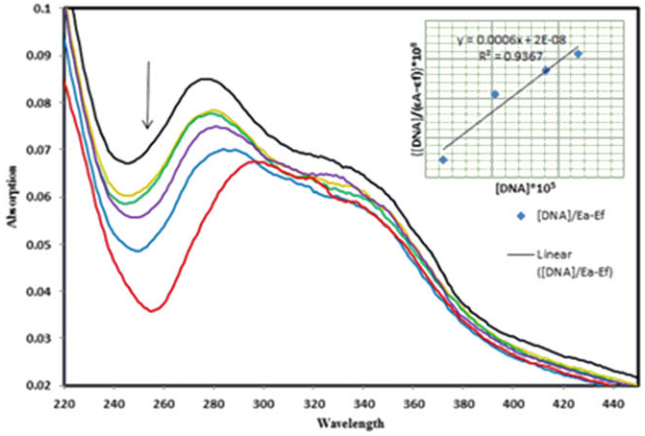

FIGURE 9 UV spectra of SP-10 (1×10^{-5} M) in the presence of increasing amounts of ct-DNA. The arrow shows the changes upon increasing amounts of ct-DNA. Inset in Fig: plot of $\frac{[DNA]}{(\varepsilon_A - \varepsilon_f)}$ *vs.*[DNA]

3.4 | DNA-binding studies of SP-10 as a potential anticancer activity

Recently investigation on the anti-cancer properties of substances has been widely considered. Therefore, studying the mechanism of interaction of substances with DNA is very important.[51,52] In this section, to gain a better understanding of the interaction between new polysubstituted pyrroles and DNA, we used UV–Visible spectroscopy, circular dichroism spectroscopy and viscosity measurements. The investigation on the interaction of a new compound with DNA is very important for the design of new drugs.[53,54] Generally, the mechanism of interactions between compounds and DNA includes a series of interactions, such as hydrogen bonding, van der Waals interactions, π-stacking interactions of aromatic heterocyclic groups between base pairs and electrostatic interactions.[55,56] The most common and effective technique used to study the interaction between DNA and compounds is the UV–Vis absorption spectroscopy.

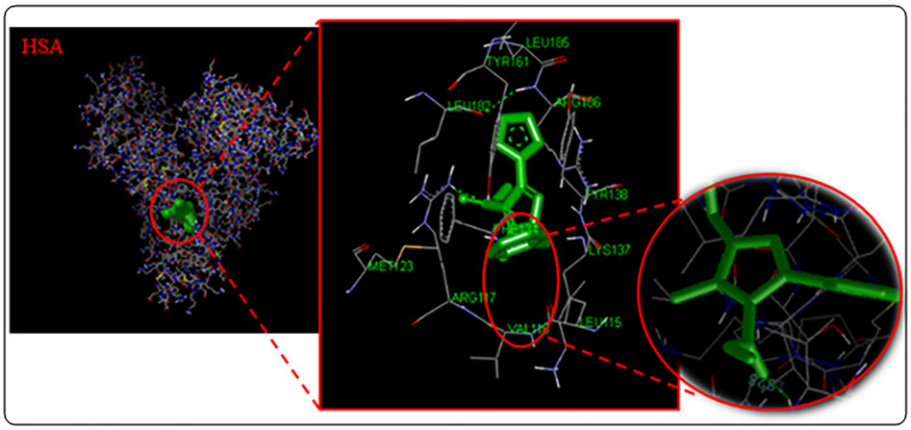

FIGURE 8 Molecular docking of the interaction of HSA with SP-10

The existence and the possible mode of interaction between compounds and DNA will be determined by the changes in the absorption intensity and the position of the spectrum bands of the compounds in UV–Vis absorption spectroscopy.[55,57] Figure 9 shows the UV–Vis absorption spectra of SP-10 (5×10^{-5} M) in the absence and presence of different concentrations of ct-DNA (0.26–2.3 $\times$ 10^{-5} M). The band centered at 241 nm exhibits a hypochromism with a moderate red shift. These results indicate that SP-10 molecules bind to ct-DNA by intercalating of their aromatic chromophore between DNA base pairs.[58,59] The binding constant of the SP-10 with ct-DNA, K_b, is calculated by the ratio of slope to the y intercept in plots $\frac{[DNA]}{(\varepsilon_A - \varepsilon_f)}$ versus [DNA] (Insets in Figure 9), according to the equation[60]:

$$\frac{[DNA]}{(\varepsilon_A - \varepsilon_f)} = \frac{[DNA]}{(\varepsilon_b - \varepsilon_f)} + \frac{1}{K_b(\varepsilon_b - \varepsilon_f)}$$

where [DNA] is the concentration of DNA in base pairs, $\varepsilon_A = A_{obsd}/[SP\text{-}10]$, ε_f = the extinction coefficient for the free SP-10 and ε_b = the extinction coefficient for the SP-10 in the fully bound form. The K_b value for interaction between SP-10 and ct-DNA was 3×10^4 M^{-1}.

The viscosity measurement study was carried out to achieve further support for the binding mode of SP-10 with ct-DNA. In general, the classic intercalation of different intercalators between the DNA base pairs causes an increase in DNA length and subsequently increases DNA viscosity.[61,62] Within this context, the viscosity of a ct-DNA solution was monitored in the presence of different concentration of SP-10 and the results show a considerable increase in the viscosity of ct-DNA upon addition of the SP-10 (Figure 10). Such a behavior may reveal the existence of intercalation binding mode between DNA and the SP-10 which may take place via

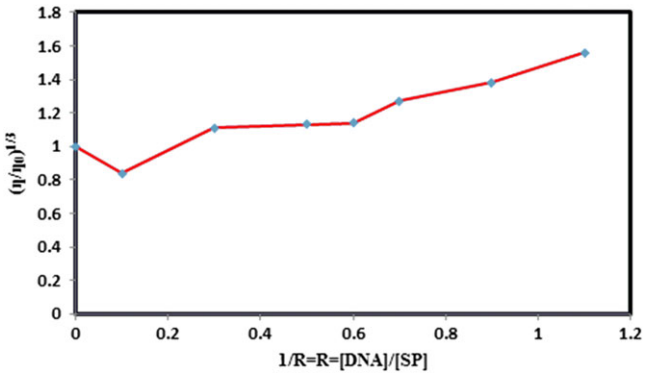

FIGURE 10 Effect of increasing concentration of SP-10 on the relative viscosity of ct-DNA at 25 °C

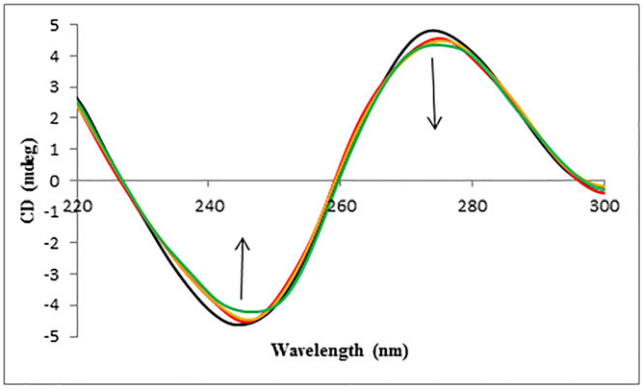

FIGURE 11 CD-spectra of the ct-DNA in the presence of different concentrations of SP-10. Conditions: c (DNA) = 8×10^{-5} M; c (SP-10) (1×10^{-5} M): 0.0, 0.9, 1.9, 2.9 and pH = 7.4

the insertion of aromatic chromophore of SP-10 between DNA base pairs.

In order to further study, the interaction mode of SP-10 with DNA and change of CD spectra of DNA in the present of SP-10 was investigated. Generally, CD spectroscopy is a useful technique in diagnosing changes in DNA morphology during drug–DNA interactions. The CD spectrum of ct-DNA exhibits a negative band at 245 nm due to the right-handed helicity of B-DNA form and a positive band at 275 nm due to base stacking which are quite sensitive to the mode of binding between small molecules and DNA.[63] The results of CD studies indicated by addition of SP-10 to a solution containing ct-DNA, CD spectra of ct-DNA in the UV region decrease in the positive and negative bands due to a transition from a more B-like to a more A-like structure (Figure 11).[64]

4 | CONCLUSION

In summary, an efficient, recoverable and reusable copper Schiff base complex immobilized on magnetic iron oxide nanoparticles was synthesized and the structural, surface, morphological and magnetic properties of resulting nanoparticles were evaluated. Covalent functionalization of complex onto the magnetic nanoparticles is successfully achieved by a multiple synthetic procedure. The catalyst also pairs the advantages of heterogeneous and homogeneous based systems, which makes it a promising material for catalytic reactions. Also, we have shown that our catalyst is an efficient, stable and strongly active nanocatalyst in one-pot four-component coupling reaction in the synthesis of pyrrole derivatives. The important features of this method include the use of cheap reagents, high yields, short reaction time, operational simplicity, and high efficiency

of the catalyst under mild conditions such as solvent free medium and room temperature. In all the reactions, turnover numbers (TON) ranging from 392 to 460 were observed. The catalyst was easily separated by a magnet and the recovered catalyst was reused for at least 10 reaction cycles without any significant loss of activity. We have also studied the binding of ct-DNA with the one of synthesized compounds here (SP-10). The different instrumental methods (absorption and viscosity measurements) suggested that the SP-10 binds to DNA via intercalation binding mode and also CD spectroscopy study inducing conformation structural changes of DNA duplex in present of SP-10. In addition, the binding affinity of SP-10 towards both ct-DNA and HSA was also investigated with molecular docking.

ACKNOWLEDGMENTS

We thank University of Tabriz and Iran National Science Foundation (INSF) (Grant Number: 95014554) for financial support to our research group.

ORCID

Behrooz Shaabani https://orcid.org/0000-0001-5576-4604
Sadegh Salehzadeh https://orcid.org/0000-0003-2840-1896

REFERENCES

[1] P. G. Cozzi, *Chem. Soc. Rev.* **2004**, *33*, 410.

[2] K. C. Gupta, A. K. Sutar, *Coord. Chem. Rev.* **2008**, *252*, 1420.

[3] T. K. Hollis, W. Odenkirk, N. P. Robinson, J. Whelan, B. Bosnich, *Tetrahedron* **1993**, *49*, 5415.

[4] I. Sheikhshoaie, A. Rezaeifard, N. Monadi, S. Kaafi, *Polyhedron* **2009**, *28*, 733.

[5] A. Ghorbani-Choghamarani, Z. Darvishnejad, M. Norouzi, *Appl. Organomet. Chem.* **2015**, *29*, 170.

[6] A. R. Judy Azar, E. Safaei, S. Mohebbi, *Mater. Res. Bull.* **2015**, *70*, 753.

[7] T. Azadbakht, M. A. Zolfigol, R. Azadbakht, V. Khakyzadeh, D. M. Perrin, *New J. Chem.* **2013**, *37*, 1.

[8] T. Tamoradi, M. Ghadermazi, A. Ghorbani-Choghamarani, *Appl. Organomet. Chem.* **2017**, e3974.

[9] N. Koukabi, E. Kolvari, A. Khazaei, M. A. Zolfigol, *Chem. Commun.* **2011**, *47*, 9230.

[10] P. D. Stevens, J. Fan, H. M. R. Gardimalla, M. Yen, Y. Gao, *Org. Lett.* **2005**, *7*, 2085.

[11] D. Gournis, M. Louloudi, M. A. Karakassides, C. Kolokytha, K. Mitopoulou, N. Hadjiliadis, *Mater. Sci. Eng. C* **2002**, *22*, 113.

[12] B. C. Gates, *Chem. Rev.* **1995**, *95*, 511.

[13] G. Grivani, S. Tangestaninejad, A. R. Halili, *Inorg. Chem. Commun.* **2007**, *10*, 914.

[14] B. Qi, X. H. Lu, S. Y. Fang, J. Lei, Y. L. Dong, D. Zhou, Q. H. Xia, *J. Mol. Catal. A Chem.* **2011**, *334*, 44.

[15] P. Li, L. Wang, L. Zhang, G. W. Wang, *Adv. Synth. Catal.* **2012**, *354*, 1307.

[16] A. Mobaraki, B. Movassagh, B. Karimi, *ACS Comb. Sci.* **2014**, *16*, 352.

[17] R. Mohammadi, M. Z. Kassaee, *J. Mol. Catal. A Chem.* **2013**, *380*, 152.

[18] R. B. N. Baig, R. S. Varma, *Chem. Commun.* **2012**, *48*, 2582.

[19] P. R. K. Murthi, D. Rambabu, M. V. B. Rao, M. Pal, *RSC Adv.* **2013**, *3*, 24863.

[20] S. Maiti, S. Biswas, U. Jana, *J. Org. Chem.* **2010**, *75*, 1674.

[21] B. L. Li, P. H. Li, X. N. Fang, C. X. Li, J. L. Sun, L. P. M. H. Zhang, *Tetrahedron* **2013**, *69*, 7011.

[22] H. Saeidian, M. Abdoli, R. Salimi, *C. R. Chim.* **2013**, *16*, 1063.

[23] F. M. Moghaddam, B. K. Foroushani, H. R. Rezvani, *RSC Adv.* **2015**, *5*, 18092.

[24] K. Konkala, R. Chowrasia, P. S. Manjari, N. L. C. Domingues, R. Katla, *RSC Adv.* **2016**, *6*, 43339.

[25] B. L. Li, M. Zhang, H. C. Hu, X. D. Z. H. Zhang, *New J. Chem.* **2014**, *38*, 2435.

[26] A. T. Khan, M. Lala, P. R. Bagdia, R. S. Basha, P. Saravanan, S. Patra, *Tetrahedron Lett.* **2012**, *53*, 4145.

[27] A. B. Atar, Y. T. Jeong, *Tetrahedron Lett.* **2013**, *54*, 5624.

[28] N. Gupta, K. N. Singh, J. Singh, *J. Mol. Liq.* **2014**, *199*, 470.

[29] S. A. Hamrahian, J. Rakhtshah, M. Mousavi, S. Salehzadeh, *Appl. Organomet. Chem.* **2018**, *32*. https://doi.org/10.1002/aoc.4501

[30] J. Rakhtshah, S. Salehzadeh, E. Gowdini, F. Maleki, S. Baghery, M. A. Zolfigol, *RSC Adv.* **2016**, *6*, 104875.

[31] J. Rakhtshah, S. Salehzadeh, *Appl. Organomet. Chem.* **2017**, 31, e3560 1-9.

[32] J. Rakhtshah, S. Salehzadeh, *Res. Chem. Intermed.* **2017**, *43*, 6973.

[33] J. Rakhtshah, S. Salehzadeh, M. A. Zolfigol, S. Baghery, *J. Coord. Chem.* **2017**, *70*, 340.

[34] M. Ma, Y. Zhang, W. Yu, H. Y. Shen, H. Q. Zhang, N. Gu, *Colloids Surf. A Physicochem. Eng. Asp.* **2003**, *212*, 219.

[35] W. Stober, A. Fink, E. J. Bohn, *J. Colloid Interface Sci.* **1968**, *26*, 62.

[36] A. D. Becke, *Phys. Rev. A* **1988**, *38*, 3098.

[37] J. P. Perdew, *Phys. Rev. B* **1986**, *33*, 8822.

[38] F. Weigend, R. Ahlrichs, *Chem. Phys.* **2005**, *7*, 3297.

[39] M. J. Frisch, G. W. Trucks, H. B. Schlegel, G. E. Scuseria, M. A. Robb, J. R. Cheeseman, J. A. J. Montgomery, T. Vreven, K. N. Kudin, J. C. Burant, J. M. Millam, S. S. Iyengar, J. Tomasi, V. Barone, B. Mennucci, M. Cossi, G. Scalmani, N. Rega, G. A. Petersson, H. M. H. Nakatsuji, M. Ehara, K. Toyota, R. Fukuda, J. Hasegawa, M. Ishida, T. Nakajima, Y. Honda, O. Kitao, H. Nakai, M. Klene, X. Li, J. E. Knox, H. P. Hratchian, J. B. Cross, C. Adamo, J. Jaramillo, R. Gomperts, R. E. Stratmann, O. Yazyev, A. J. Austin, R. Cammi, C. Pomelli, J. W. Ochterski, P. Y. Ayala, K. Morokuma, G. A. Voth, P. Salvador, J. J.

Dannenberg, V. G. Zakrzewski, S. Dapprich, A. D. M. C. Daniels, O. Strain, D. Farkas, K. Malick, A. D. Rabuck, K. Raghavachari, J. B. Foresman, J. V. Ortiz, Q. Cui, A. G. Baboul, S. Clifford, J. Cioslowski, B. B. Stefanov, G. Liu, A. Liashenko, P. Piskorz, I. Komaromi, R. L. Martin, D. J. Fox, T. Keith, M. A. Al-Laham, C. Y. Peng, A. Nanayakkara, M. Challacombe, P. M. W. Gill, B. Johnson, W. Chen, M. W. Wong, C. Gonzalez, J. A. Pople, *Gaussian software*, Gaussian, Inc, Pittsburgh, PA **2003**.

[40] G. M. Morris, D. S. Goodsell, R. S. Halliday, R. Huey, W. E. Hart, R. K. Belew, A. J. Olson, *Autodock, version 4.0.1 The Scripps Research Institute*, La Jolla, CA **2007**.

[41] S. Rezaei, A. Ghorbani-Choghamarani, R. Badri, *Appl. Organomet. Chem.* **2016**, *30*, 985.

[42] X. Le, Z. Dong, Z. Jin, Q. Wang, J. Ma, *Catal. Commun.* **2014**, *53*, 47.

[43] Q. Du, W. Zhang, H. Ma, J. Zheng, B. Zhou, Y. Li, *Tetrahedron* **2012**, *68*, 3577.

[44] R. Abu-reziq, H. Alper, D. S. Wang, M. L. Post, *J. Am. Chem. Soc.* **2006**, *128*, 5279.

[45] Z. Moradi-Shoeili, M. Zare, M. Bagherzadeh, S. Özkar, S. Akbayrak, *J. Coord. Chem.* **2016**, *69*, 668.

[46] N. Hosseinpour Moghadam, S. Salehzadeh, N. Shahabadi, *Nucleosides Nucleotides Nucleic Acids* **2017**, *36*, 553.

[47] S. Salehzadeh, F. Hajibabaei, N. Hosseinpour Moghadam, S. Sharifinia, S. Khazalpour, R. Golbedaghi, *J. Fluoresc.* **2018**, *28*, 195.

[48] W. He, Y. Li, J. Tian, H. Liu, Z. Hu, X. Chen, *J. Photochem. Photobiol. A.* **2005**, *174*, 53.

[49] F. Janati Fard, Z. Mashhadi Khoshkhoo, H. Mirtabatabaei, M. R. Housaindokht, R. Jalal, H. Eshtiagh Hosseini, M. R. Bozorgmehr, A. A. Esmaeili, M. Javan Khoshkholgh, *Spectrochim. Acta A* **2012**, *97*, 74.

[50] H. Dezhampanah, R. Firouzi, *J. Biomol. Struct. Dyn.* **2017**, *35*, 3615.

[51] F. Karimi Dermani, M. Saidijam, R. Amini, A. Mahdavinezhad, K. Heydari, R. Najafi, *J. Cell. Biochem.* **2017**, *118*, 1547.

[52] S. Karimi, A. Mohamadnia, S. A. Nadji, R. Yadegarazari, A. Khosravi, N. Bahrami, M. Saidijam, *Iran. Biomed. J.* **2015**, *19*, 17.

[53] J. W. Lown, *Anticancer Drug Des.* **1998**, *3*, 25.

[54] M. P. Singh, T. Joseph, S. Kumar, Y. Bathini, J. W. Lown, *Chem. Res. Toxicol.* **1992**, *5*, 597.

[55] M. Sirajuddin, S. Ali, A. Badshah, *J. Photochem. Photobiol. B* **2013**, *124*, 1.

[56] T. Topala, A. Bodoki, L. Oprean, R. Oprean, *Farmacia* **2014**, *62*, 6.

[57] F. Dimiza, A. N. Papadopoulos, V. Tangoulis, V. Psycharis, C. P. Raptopoulou, D. P. Kessissoglou, G. Psomas, *Dalton Trans.* **2010**, *39*, 4517.

[58] A. M. Pyle, J. P. Rehmann, R. Meshoyrer, C. V. Kumar, N. J. Turro, J. K. Barton, *J. Am.Chem. Soc.* **1989**, *111*, 3053.

[59] F. Dimiza, A. N. Papadopoulos, V. Tangoulis, V. Psycharis, C. P. Raptopoulou, D. P. Kessissoglou, G. Psomas, *J. Inorg. Biochem.* **2012**, *107*, 54.

[60] A. Wolfe, G. H. Shimer, T. Meehan, *Biochemistry* **1987**, *26*, 6392.

[61] J. L. Zhou, Z. M. Qian, Y. D. Luo, D. Tang, H. Chen, L. Yi, P. Li, *Biomed. Chromatogr.* **2008**, *22*, 1164.

[62] N. Shahabadi, F. Shiri, M. S. Norouzibazaz, A. Falah, *Nucleosides Nucleotides Nucleic Acids* **2018**, *20*, 1.

[63] M. P. Uma, M. J. Palaniandavar, *Inorg. Biochem* **2004**, *98*, 219.

[64] N. Shahabadi, N. Hosseinpour Moghadam, *J. Lumin.* **2013**, *134*, 629.

SUPPORTING INFORMATION

Additional supporting information may be found online in the Supporting Information section at the end of the article.

How to cite this article: Rakhtshah J, Shaabani B, Salehzadeh S, Hosseinpour Moghadam N. The solvent-free synthesis of polysubstituted pyrroles by a reusable copper Schiff base complex immobilized on silica coated Fe_3O_4, and DNA binding study of one resulting derivative as a potential anticancer drug. *Appl Organometal Chem*. 2018;e4754. https://doi.org/10.1002/aoc.4754